Gao et al. Nanoscale Research Letters (2016) 11:496
DOI 10.1186/s11671-016-1718-9

Nanoscale Research Letters

NANO EXPRESS Open Access

Photodegradation of Unsymmetrical Dimethylhydrazine by TiO_2 Nanorod Arrays Decorated with CdS Nanoparticles Under Visible Light

Xin Gao[1], Xiangxuan Liu[1], Xuanjun Wang[1], Zuoming Zhu[2], Zheng Xie[1*] and Jun Li[1]

Abstract

Photocatalysis technology could utilize solar energy to degrade many toxic pollutants and provides possibility to deal with unsymmetrical dimethylhydrazine (UDMH) wastewater with less energy consumption. In this study, well-aligned TiO_2 nanorod arrays (TiO_2 NRAs) were grown directly on transparent conductive glass (FTO) via a hydrothermal method, and TiO_2 NRAs/CdS heterostructure films were prepared by decorating TiO_2 NRAs with CdS nanoparticles through successive ion layer adsorption and reaction (SILAR). Under visible light, the TiO_2 NRAs/CdS heterostructure displays enhanced photodegrading capacity compared with the bare TiO_2 NRAs, and the highest photodegradation rate, 27.5% higher than that of the bare TiO_2 NRAs, was achieved by the sample with 15 SILAR cycles. Additionally, the solution pH had some influence on the degradation process, which shows that the best degradation rate can be achieved in the neutral solution (pH is ca. 7.2), and the photodegradation process can be better in alkaline solution than in the acid solution. Moreover, the visible photocatalytic stability of the TiO_2 NRAs/CdS sample was investigated. Finally, the underlying photocatalytic mechanism was discussed according to the photoelectrochemical and photoluminescence results.

Keywords: TiO_2 nanorod arrays, CdS nanoparticle, Photocatalysis, Visible light, Unsymmetrical dimethylhydrazine

Background

Unsymmetrical dimethylhydrazine (UDMH) is primarily used as a high-energy propellant [1]. However, as an eco-toxicant, UDMH greatly endangers human health once occurred in water under natural condition. Traditional water treatment methods, such as chlorination, ozone oxidation, and catalytic oxidation with oxygen and hydrogen peroxide in the presence of Cu, Fe, and Co salts supported on zeolites as catalysts, achieve satisfactory degrading results, but the high energy consumption (continuous need for an oxidizing agent such as hydrogen peroxide and ozone) and complexity of the recycle of the catalyst make these methods inefficient for applications. Recently, cavitational decontamination of UDMH wastewater seems attractive. Even though it is an oxidant-free method, much energy is still needed to form gas bubbles in the liquid and then explosively develop, grow large, and, at last, collapse [1]. Therefore, it is urgent to develop an energy-efficient method to remove UDMH from water. It is reported that photocatalyst titanium oxide (TiO_2) is non-selective during degradation of organic compounds [2]. A lot of researches have been made to degrade various organic contaminants and got excellent degrading results [3–9]. In this respect, using TiO_2 as a photocatalyst to degrade UDMH may be an energy-saving manner.

Furthermore, TiO_2 is abundant, low cost, nontoxic, and highly resistant to photocorrosion [10]. Once inspired, the generated electron and hole pairs (e^-/h^+) migrate to the surface of TiO_2 for a direct oxidation of the polluting species or undergo redox reactions [11] at the surface of the semiconductor to form extremely reactive oxygen species (·OH, O_2·, H_2O_2, O_3, etc.) and then degrade the pollutions [12]. In particular, regular one-dimensional TiO_2, with efficient and tunable optical

* Correspondence: xiezheng10@tsinghua.org.cn
[1]High-Tech Institute of Xi'an, Shaanxi 710025, China
Full list of author information is available at the end of the article

absorption as well as low reflectivity [13], exhibits good performance due to the unique nanostructure, which facilitates the effective separation of the photoexcited carriers.

However, the band gap (3.0~3.2 eV) of TiO_2 is too wide to efficiently absorb visible light, which is the main component of the solar spectrum (ca. 43%) [14]. One of the promising strategies to overcome this drawback is to couple TiO_2 with other narrow band gap semiconductors capable of harvesting the photons in the visible light region [15]. CdS with a band gap of ca. 2.2–2.4 eV [16] has been one of the most intensively studied narrow band gap semiconductors to improve the visible light absorption of TiO_2. Moreover, the good match of band positions between TiO_2 and CdS ensures efficient separation of charge carriers [17, 18].

So far, few researches are reported in dealing with UDMH wastewater by semiconductor photocatalysis. Most of the reported researches are conducted under UV irradiation and use powder catalysts. Here, we prepared visible light-induced TiO_2 nanorod arrays (TiO_2 NRAs) decorated with CdS thin films and applied the obtained photocatalyst for the degradation of UDMH under visible light irradiation. To the best of our knowledge, research on one-dimensional TiO_2 NRAs decorated with CdS to degrade UDMH under visible light irradiation has not been reported. Compared with the bare TiO_2 NRAs, TiO_2 NRAs/CdS exhibited dramatically enhanced photocatalytic capacity. By adjusting the amount of CdS deposited on the TiO_2 NRAs, the degrading rate can be improved significantly. The effect of pH of wastewater on the degrading rate was investigated. Finally, photoelectrochemical performance and photoluminescence (PL) spectra were measured to clarify the photocatalytic mechanism.

Methods

Synthesis of TiO_2 Nanorod Arrays Decorated with CdS

Vertically aligned TiO_2 NRAs were prepared on transparent fluorine-doped tin oxide (FTO) glass substrates (14 Ω/sq) using the hydrothermal method based on our published procedure [19]. Deionized water (DI, 10 mL) was mixed with hydrochloric acid (10 mL, 36.8 wt%) and stirred for 5 min before tetrabutyl titanate (0.4 mL, 98%) was added. When the solution was stirred to clear clarification, the mixture solution was transferred to a Teflon-lined stainless steel autoclave. Clean FTO substrates (area 4.5 cm^2) were immersed with the conducting side face down. The autoclave was put in an oven at a temperature of 150 °C and taken out from the oven after 5 h. After the autoclave was cooled to room temperature, the FTO substrate was rinsed with DI water and dried naturally at room temperature.

CdS nanoparticles were deposited on TiO_2 nanorod arrays through a successive ion layer adsorption and reaction (SILAR) method according to the experimental procedure reported by Xie et al. [20] with a slight modification. Briefly, the TiO_2 NRAs substrate was dipped in a 0.01 M $Cd(NO_3)_2$ aqueous solution for 30 s, rinsing it with DI water for 30 s, and then immersed into a 0.01 M Na_2S aqueous solution for another 30 s, and rinsing it again with DI water for 30 s. The SILAR process was repeated to obtain TiO_2 NRAs sensitized with different amounts of CdS nanoparticles, which were designated as TiO_2 NRAs/CdS (*n* cycles).

Characterization

The surface morphology was obtained with a scanning electron microscopy (SEM, VEDAIIXMUINCN) equipped with an energy-dispersive X-ray spectroscopy (EDS) system. Waster 5510 transmission electron microscopy (TEM) was used to further characterize the film microstructure. X-ray diffraction (XRD, PANalytical) with Cu-Kα ($\lambda = 0.15401$ nm) was operated at 40 kV and 40 mA in a 2θ range of 20°–80° at a scanning speed of 5° min^{-1}. Raman spectra were recorded using an inVia Reflex Raman spectrometer under Ar^+ (532 nm) laser excitation at room temperature. The optical properties were probed by a UV–vis spectrophotometer (UV1800, Shimadzu) with FTO substrate as a blank. X-ray photoelectron spectroscopy (XPS) was obtained using ESCALAB 250Xi (The binding energy of the XPS spectra was calibrated with reference to the C 1s peak at 284.8 eV.)

Photoelectrochemical measurements were performed in a 250-mL quartz cell using a three-electrode configuration, including the prepared sample as a working electrode, a Pt foil as a counter electrode, a saturated Ag/AgCl as a reference electrode, and 0.1 M Na_2S as an electrolyte. The working electrode was illuminated within an area of about 1.5 cm^2 at zero bias voltage versus the Ag/AgCl electrode under solar-simulated (AM 1.5 G filtered, 100 mW cm^{-2}, CEL-HXF300) light sources with a UV cutoff filter (providing visible light with $\lambda \geq 420$ nm). The photoluminescence (PL) spectra for solid samples were recorded on a Fluoromax-4 spectrophotometer with an excitation wavelength at 350 nm.

Photocatalytic Degradation of UDMH

The photodegradation of UDMH aqueous solution was carried out in an open reactor under visible light irradiation. The TiO_2 NRAs/CdS films (area about 6 cm^2) were immersed in UDMH aqueous solution (15 mL) with an initial concentration of 20 mg L^{-1}. Then, dark (adsorption) experiments were carried out for 30 min to reach the adsorption equilibrium of UDMH with the TiO_2 NRAs/CdS film. The film-coated side of the substrate was exposed to the light source, and the light source was a

300-W xenon lamp with visible light illumination of 60 mW cm^{-2}; an ultraviolet cutoff filter was used to exclude UV light with a wavelength below 420 nm. Traces of UDMH can react with amino ferrocyanide sodium to form a red complex in a weakly acidic aqueous solution, and the color depth of the red complex is proportional to the content of UDMH. So, the concentration of UDMH left in the aqueous system can be measured by a spectrophotometer at 500 nm which is the characteristic absorption wavelength of the red complex. The procedure is as follows: (1) UDMH aqueous solution (0.5 mL) was added to a test tube with a volume of 50 mL and then diluted to 25 mL by DI water. (2) Buffer solution (1 mL) was added to adjust the above solution to a weakly acidic aqueous solution. The buffer solution was made of citric acid and disodium hydrogen phosphate with a pH of about 4.8. (3) Amino ferrocyanide sodium (1 mL, 1.5 g L^{-1}) was added to the test tube, and then, the test tube was placed in 30 °C water bath for 1 h. (4) The final red complex solution was measured by a spectrophotometer at 500 nm. The relative concentration of UDMH in the solution was derived by comparing its absorption intensity with the standard curve line.

Results and Discussion

The XRD patterns of TiO_2 NRAs/CdS are shown in Fig. 1a. The characteristic peaks at $2\theta = 36.078°$, 62.750°, 69.010°, and 69.795° can be indexed to rutile TiO_2 (PDF No. 21-1276). Other peaks are attributed to the FTO substrate. There is no characteristic peak for CdS after SILAR, and the absence of diffraction peak associated with CdS might be due to the low concentration and the well dispersion of CdS in the nanocomposite. To further confirm the presence of CdS, we measured the bare TiO_2 NRAs and the TiO_2 NRAs/CdS (20 cycles) samples with the glancing angle X-ray diffraction (GXRD) method. The GXRD measurement was performed with a scanning step of 0.02° and a dwell time of 0.15 s in the scanning range of 22°–32°. The corresponding GXRD pattern is shown in the inset of Fig. 1a. It can be seen that only the TiO_2 NRAs/CdS (20 cycles) sample displays one peak at about 26.5°, which is corresponding to CdS (111) (PDF No. 10-0454) and confirms the successful deposition of CdS on TiO_2 NRAs.

Raman microscopy was conducted to further identify the presence and crystallinity of CdS, and the results are displayed in Fig. 1b. The peak at 117 cm^{-1} is due to

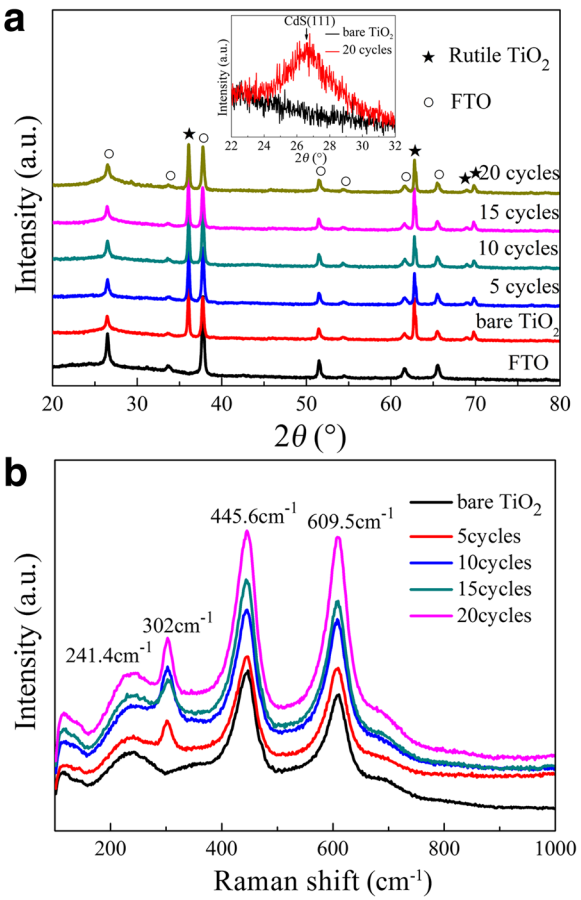

Fig. 1 **a** XRD patterns and **b** Raman spectra of TiO_2 NRAs/CdS

plasma emission of the Ar^+ laser [21]. The three strong Raman peaks located around 241.4, 445.6, and 609.5 cm^{-1} should be assigned to the Raman active modes of rutile TiO_2 [22], which is consistent with the XRD patterns. The well-resolved band located at ~302 cm^{-1} is from CdS [23], which is in accordance with the first-order scattering of the longitudinal optical phonon mode [24].

To further reveal the valence states and surface chemical compositions of the composite, XPS is employed to characterize the TiO_2 NRAs/CdS (15 cycles) sample. Figure 2a confirms Ti, O, Cd, S, and C are present in the nanocomposite. In Fig. 2b, two peaks for the Ti 2p are observed (464.29 eV for Ti $2p_{1/2}$ and 458.59 eV for Ti $2p_{3/2}$). These values are in good agreement with the XPS data known for Ti^{4+} in TiO_2 [25]. The high-resolution spectrum of O 1s in Fig. 2c shows two components by Gaussian curve fittings. The pronounced peak at 529.76 eV is attributed to the lattice oxygen of TiO_2, and the other peak at 531.33 eV is attributed to oxygen defect (i.e., Ti–OH) [26]. It is reported that oxygen defect may play an important role in enhancing the photocatalytic activity [27]. Two bands at 405.17 and 411.92 eV are observed in Fig. 2d, which can be ascribed to the Cd $3d_{5/2}$ and Cd $3d_{3/2}$ binding energies, respectively. The result is accordance with the previous report of Cd^{2+} values [28]. Moreover, XPS peaks of S 2p located at 161.45 and 162.57 eV should be assigned to the spectra of S $2p_{1/2}$ and S $2p_{3/2}$, respectively, indicating that the composite electrode contains S^{2+} of CdS [29]. As to the high-resolution spectrum of O 1s shown in Fig. 2f, the peak at 284.80 eV is from adventitious carbon (C–C/C–H bonds), which is inevitable in XPS measurement [30], while the peaks at 286.23 and 288.42 eV may be due to the formation of carbonate species [31, 32]. From the above analysis, one can clearly see that CdS is successfully deposited on the TiO_2 NRAs.

The top-view SEM image of the bare TiO_2 NRAs is shown in Fig. 3a. It can be seen that the nanorods are uniform with a rectangular cross section and the nanorod diameter is around 60~120 nm. The corresponding cross section image (in Fig. 3b) shows that vertically or slantingly aligned nanorod arrays are uniformly grown in high density on the FTO substrate and the typical nanorod length was about 2.2 μm. From Fig. 3b–f, it can be

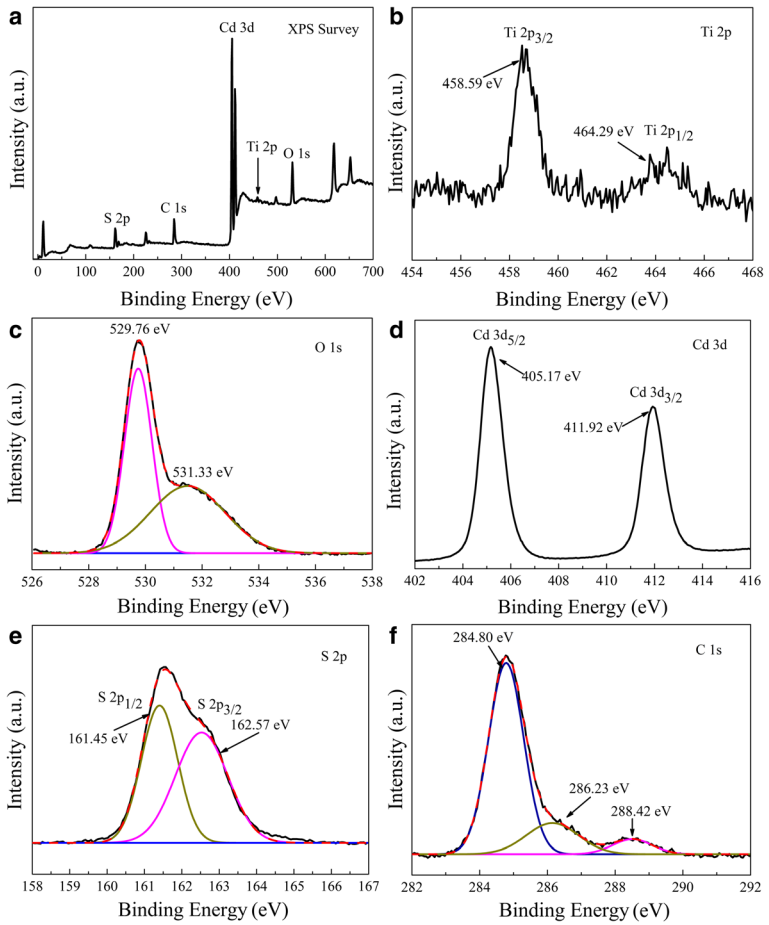

Fig. 2 **a** XPS survey spectrum of TiO_2/CdS (15 cycles) and high-resolution XPS spectra of **b** Ti 2p, **c** O 1s, **d** Cd 3d, **e** S 2p, and **f** C 1s

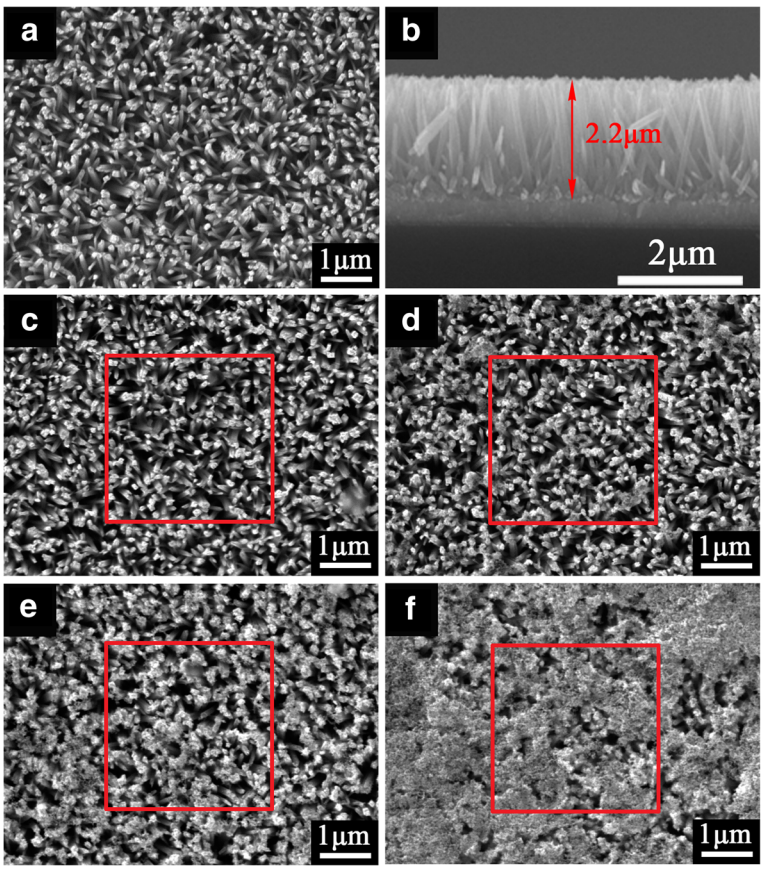

Fig. 3 SEM images of TiO_2 NRAs/CdS: **a** 0, **c** 5, **d** 10, **e** 15, and **f** 20 SILAR cycles. **b** The corresponding cross section image of **a**

seen that the amount of CdS accumulated gradually with increase in SILAR cycles. Especially when TiO_2 NRAs were decorated with CdS by 20 cycles (in Fig. 3f), the entire surface of the TiO_2 NRAs was almost covered by a film consisting of larger CdS crystallites. EDS analysis was also carried out for areas marked by the red rectangles in Fig. 3. The results are shown in Additional file 1: Figure S1. It is observed that the Ti/Cd ratio was from ~23.94 to ~3.31 when the SILAR cycles increased from 5 to 20 cycles, which indicates that more CdS NPs were deposited on TiO_2 NRAs with a higher number of SILAR cycles.

The morphology of TiO_2 NRAs/CdS was further investigated by TEM. From Fig. 4a, c, e, it can be seen that the diameter of the nanorod in all of the samples is consistent with the result in SEM images. The corresponding high-resolution TEM images all show the lattice fringes of rutile TiO_2. From the TEM images of the TiO_2 NRAs/CdS (5 cycles) in Fig. 4c, d, no obviously recognizable CdS NPs on the surface of the nanorods can be found due to the low content of CdS after only 5 cycles' deposition. However, Additional file 1: Figure S1 (a) displays the existence of CdS in the TiO_2 NRAs/CdS (5 cycles) sample. When the SILAR deposition increased to 15 cycles shown in Fig. 4e, f, it can be seen that the smooth surface of the bare TiO_2 NRAs become rough after the deposition of CdS. A thin layer made of CdS particles covered the whole nanorod as shown in Additional file 2: Figure S2. The high-resolution TEM image in Fig. 4f gives a lattice fringe of about 0.332 nm, corresponding to the *d* (111) space of CdS.

The optical absorption property of TiO_2 NRAs decorated with CdS NPs is shown in Fig. 5. The inset photograph is the image of the TiO_2 NRAs/CdS NPs, showing clearly the color change with different SILAR cycles. With the deposition of CdS NPs, light absorption of TiO_2 NRAs was strengthened from 400 to 500 nm. The more CdS are deposited, the stronger the visible light absorption capacity is. It is reported that any red shift in optical response of TiO_2 toward the longer wavelength region gives the possibility of higher photocatalytic activity [33]. Tiny absorption of the as-prepared TiO_2 sample in the visible light range was found. This abnormal phenomenon can be attributed to the scattering of light caused by the nanorod arrays as well as the absorption by the FTO itself [29, 34].

Photodegradation of UDMH was carried out under visible light irradiation ($\lambda \geq 420$ nm) using the CdS-decorated

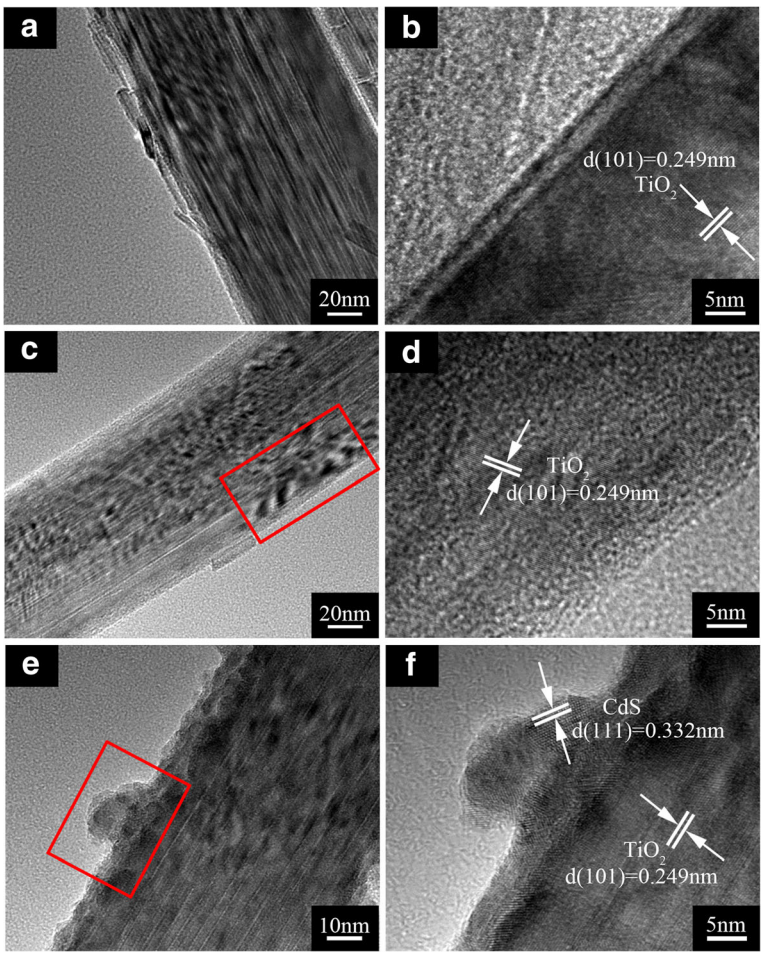

Fig. 4 TEM images. **a**, **b** The bare TiO_2 NRAs. **c**, **d** TiO_2 NRAs/CdS (5 cycles). **e**, **f** TiO_2 NRAs/CdS (15 cycles)

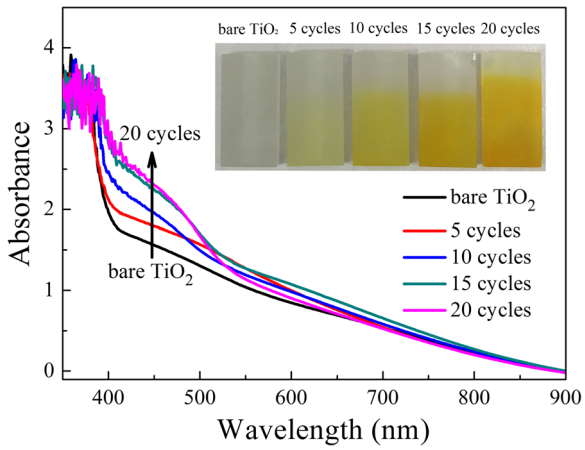

Fig. 5 Absorption spectra of TiO_2 NRAs/CdS. *Inset* is the optical photograph of TiO_2 NRAs/CdS

TiO_2 NRAs as a photocatalyst. In Fig. 6a, with the extension of the visible light irradiation time, one can see that the degradation rates of UDMH by different photocatalysts increased. Without the addition of any catalysts under visible light irradiation for 180 min, the degradation rate of UDMH was only 2.18%, which indicated that the degradation ability by simple visible light was very low, while the bare TiO_2 NRAs could achieve 7.86% under the same condition. Enhancement could be observed by using the CdS-decorated TiO_2 NRAs as the photocatalyst. For example, the degradation rate was 19.56% by TiO_2 NRAs/CdS (5 cycles), and it could reach 36.77% if using TiO_2 NRAs/CdS (15 cycles). However, continually increasing the SILAR cycles to 20, the degradation rate decreased (i.e., it was down to 27.95%) instead of getting higher. It can be seen that the degradation rate of UDMH first increased with the increase of the CdS deposition cycles and then decreased when the CdS deposition cycles continually increased. Thus, we may deduce that when a proper amount of CdS NPs are decorated, more visible light could be absorbed to produce more excited carriers and the carriers could be separated more

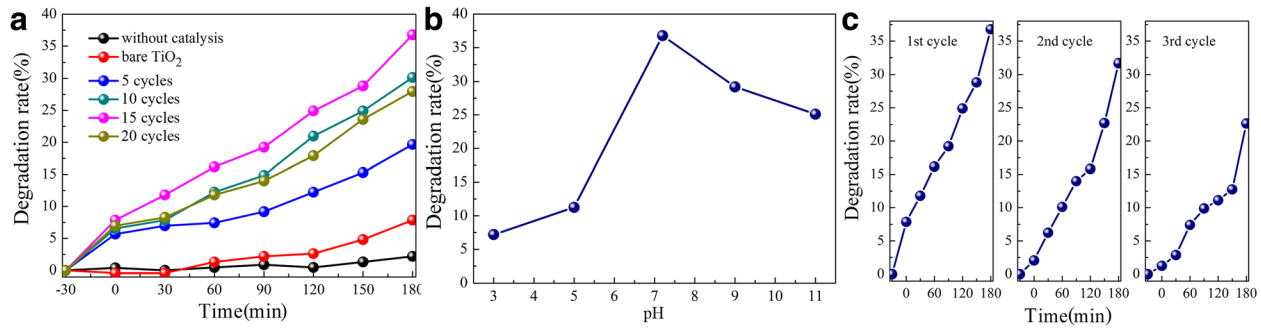

Fig. 6 **a** Degradation rate of UDMH by TiO_2 NRAs/CdS with different SILAR cycles. **b** Influence of different pH on the degradation rate of UDMH. **c** Cyclic photodegradation of UDMH with TiO_2 NRAs/CdS (15 cycles)

efficiently, which lead to higher degradation rates. However, excess deposition of CdS NPs in the TiO_2 NRAs/CdS (20 cycles) sample causes a longer transport path for the photogenerated electron–hole pairs [15, 35], and it is a potential barrier for charge carrier transfer. This is not beneficial for the effective separation of carriers, therefore leading to the decrease of the photodegradation rate. A proper amount of CdS decoration is the key factor that decides the photodegradation efficiency.

The influence of pH on the degradation rate of UDMH was also studied, and pH of the simulated UDMH solution was adjusted to 3, 5, 9, and 11 by NaOH and H_2SO_4. In this experiment, TiO_2 NRAs decorated with CdS NPs by 15 SILAR cycles were chosen as the catalyst. It was discovered that the best degradation rate of UDMH could be achieved in the neutral solution (pH is c.a. 7.2). The photocatalytic degradation rate of UDMH under alkaline circumstance is better than that under acid circumstance.

Durability is another important point of CdS-related photocatalyst because CdS may cause photocorrosion under irradiation. The visible photocatalytic durability of the TiO_2 NRAs/CdS (15 cycles) sample was investigated and displayed in Fig. 6c. The photodegradation ratio of UDMH after each 180-min irradiation for 3 cycles was about 36.77, 31.69, and 22.63%, respectively. Photocorrosion effect led to more than 35% decrease of the degradation rate after three runs. It means that part of Cd^{2+} was left in the aqueous solution which could result in the second pollution, the most pressing problem about CdS-related photoactivity. However, for the excellent photoconversion of CdS, it still attracts intensive studies by lots of researchers. In our previous experiment [36], $NiFe_2O_4$-modified TiO_2 NRAs were used in the photodegradation of UDMH wastewater under the same condition; however, the degrading rate (c.a. 22.06%) was relatively low compared with that of CdS-modified TiO_2 NRAs. In this case, we would be committed to improve the durability of TiO_2 NRAs/CdS in the future.

A proposed model for the photodegradation activity can be illustrated as follows. When TiO_2 NRAs/CdS is irradiated by visible light ($\lambda \geq 420$ nm), CdS could be effectively excited to produce electron and hole pairs. As the conduction band (CB) of TiO_2 is more positive than that of CdS, the excited electrons immigrate from the CB of CdS to the CB of TiO_2. Thus, the photoinduced charge carriers can be effectively separated, and the lifetime is prolonged. The accumulated electrons (e^-) in the CB of TiO_2 could react with dissolved oxygen molecules to form superoxide radical anions ($\cdot O_2-$) [37], which could be further reduced to highly reactive hydroxyl radicals ($\cdot OH$) [38]. The positive holes in the valence band (VB) of CdS can also be trapped by OH^- to produce $\cdot OH$ species [39]. These strong oxidizing free radicals then react with UDMH. Under acid circumstance, abundant H^+ existing in the resolution may hinder process (3), while under alkaline circumstance, OH^- existing in the resolution may be in favor of process (4); this may account for the effect of the pH on the degrading rate.

$$\mathrm{CdS} + \mathrm{hv(visible)} \rightarrow \mathrm{CdS}\left(e_{\mathrm{cb}}^- + h_{\mathrm{vb}}^+\right) \quad (1)$$

$$\mathrm{CdS}\left(e_{\mathrm{cb}}^- + h_{\mathrm{vb}}^+\right) + \mathrm{TiO_2} \rightarrow \mathrm{CdS}\left(h_{\mathrm{vb}}^+\right) + \mathrm{TiO_2}\left(e_{\mathrm{cb}}^-\right) \quad (2)$$

$$h_{\mathrm{vb}}^+ + \mathrm{H_2O} \rightarrow \cdot\mathrm{OH} + \mathrm{H}^+ \quad (3)$$

$$h_{\mathrm{vb}}^+ + \mathrm{HO}^- \rightarrow \cdot\mathrm{OH} \quad (4)$$

$$\mathrm{TiO_2}\left(e_{\mathrm{cb}}^-\right) + \mathrm{O_2} \rightarrow \mathrm{TiO_2} + \cdot\mathrm{O_2}^- \quad (5)$$

$$\cdot\mathrm{OH} + \mathrm{UDMH} \rightarrow \text{degradation products} \quad (6)$$

$$\cdot O_2^- + \mathrm{UDMH} \rightarrow \text{degradation products or} \quad \cdot O_2^- + H^+ \rightarrow HO_2\cdot \rightarrow \rightarrow \cdot OH \qquad (7)$$

To better understand the photocatalytic performance of the TiO_2 NRAs/CdS, photocurrent intensity versus potential (I–V) and PL measurements were carried out.

Figure 7a shows the I–V curves measured for TiO_2 NRAs/CdS. Under visible light irradiation, the bare TiO_2 NRAs electrode showed little photocurrent density. After the deposition of CdS, the photocurrent density of the samples increased remarkably. A higher photocurrent density indicates a higher efficiency in the separation of electrons and holes [40], thus suggesting a better photocatalytic performance. In Fig. 7a, the photocurrent density first increased with the increase of the CdS NPs deposited from 5 to 15 cycles. However, when the deposition of CdS reached to 20 cycles, the photocurrent density was significantly decreased rather than continuing to increase. Though more CdS NPs brought the increased harvesting of photons, it did not lead to the continual increase of the photocurrent density. Two points may account for this phenomenon. Firstly, excess CdS deposition made the CdS crystallites larger, which increased the transfer path for the photogenerated carriers [15, 35] and thus hindered the fast transport of the carriers. Secondly, when the SILAR deposition increased to 20 cycles, the abrupt increase of CdS nanoparticles would create more defects, which could act as recombination centers [29]. The two points both result in the ineffective separation of the carriers. In addition, Fig. 7a also shows that the open circuit potential (V_{oc}) for TiO_2 NRAs become more negative after decorated with CdS (−0.26 V for the bare TiO_2 NRAs, −1.13, −1.17, −1.23, and −1.21 V for TiO_2 NRAs decorated by 5, 10, 15, and 20 cycles, respectively). It is reported that more negative V_{oc} means better charge carrier separation [41, 42], thus leading to better photocatalytic capacity.

The PL technique is an effective way to explore the separation of the charge carriers [29]. Figure 7b demonstrates the PL spectra of the CdS-decorated TiO_2 NRAs, which are excited at a wavelength of 350 nm. The peak in the PL spectra originates from the recombination of the photogenerated electron–hole pairs [29, 43]. The higher the PL intensity is, the higher the recombination rate of the carriers is [43, 44]. It is clear to see that a broad emission peak centered at around 450 nm was observed for all the samples. With the SILAR cycles increased to 15 cycles, the intensity of the emission peak is quenched drastically. This indicates that the introduction of CdS brings more effective separation of the photoinduced electron–hole carrier pairs, the prolonged lifetime of the carriers, and thereby the less recombination rate of the photogenerated electron and holes in the TiO_2/CdS nanocomposite [45]. However, continually increasing the SILAR to 20 cycles, there would be an abrupt increase of CdS nanoparticles to form defects. These defects could act as recombination centers for the photoinduced carriers [29, 46], thus initiating the rapid photoelectron–hole recombination within CdS [47] and therefore causing a stronger PL intensity.

From the I–V curves and PL spectra, it can be seen that a proper amount of CdS decoration makes more effective charge carrier separation, which will then play an important role in the following photocatalytic degrading activity.

Conclusions

The CdS NP-decorated TiO_2 NRAs were synthesized and applied for the photodegradation of UDMH under visible light irradiation. Compared with the bare TiO_2 NRAs, TiO_2 NRAs/CdS heterojunction exhibited enhanced photocatalytic capacity toward UDMH. By adjusting the cycles of SILAR, TiO_2 NRAs decorated by 15 cycles of CdS got the best degradation efficiency of UDMH. Besides, it seems that alkaline circumstance is more beneficial for the photocatalytic degradation of UDMH than acid circumstance. When the pH of the simulated UDMH wastewater was about 7.2, the degradation rate of UDMH was highest. Through I–V

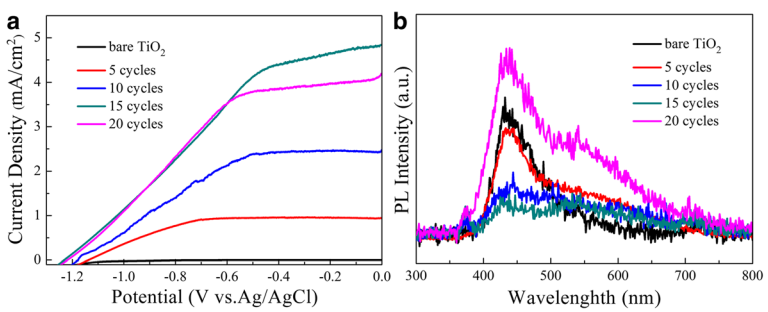

Fig. 7 **a** Photocurrent intensity versus potential characteristics of the TiO_2 NRAs/CdS NPs. **b** PL spectra of TiO_2/NRAs CdS NPs excited by 350 nm

and PL characterization, the proposed photocatalytic mechanism was further confirmed. The synergetic effect between CdS and TiO_2 leads to high electron injection efficiency and fast electron transfer; thus, the photocatalytic capacity of TiO_2 NRAs/CdS can be enhanced significantly. This research proved that photocatalysis may be a possible way to deal with the toxic UDMH wastewater with low energy consumption and easy recycle of the catalyst.

Additional files

Additional file 1: Figure S1. EDS images of TiO_2 NRAs/CdS. (a) 5 cycles, (b) 10 cycles, (c) 15 cycles, and (d) 20 cycles. (448 KB)

Additional file 2: Figure S2. TEM image of TiO_2 NRAs/CdS (15 cycles). (964 KB)

Abbreviations

CB: Conduction band; DI: Deionized water; EDS: Energy-dispersive X-ray spectroscopy; FTO: Fluorine-doped tin oxide; GXRD: Glancing angle X-ray diffraction; *I–V*: Photocurrent intensity versus potential; NPs: Nanoparticles; PL: Photoluminescence; SILAR: Successive ion layer adsorption and reaction; TEM: Transmission electron microscopy; TiO_2 NRAs: TiO_2 nanorod arrays; UDMH: Unsymmetrical dimethylhydrazine; VB: Valence band; V_{oc}: Open circuit potential; XPS: X-ray photoelectron spectroscopy; XRD: X-ray diffraction

Acknowledgements

The authors are highly grateful to Mr. Zhaobin She for the kind help during the film characterization, especially the SEM.

Funding

There is no funding supported.

Authors' Contributions

XG conceived and carried out the experiments, conducted the studies, made the processing and analysis of the data, and wrote the manuscript. ZX and ZZ participated in the discussion and revised the manuscript. XL and XW supervised the research work. JL made some characterization in the experiment. All authors read and approved the final manuscript.

Competing Interests

The authors declare that they have no competing interests.

Author details

[1]High-Tech Institute of Xi'an, Shaanxi 710025, China. [2]High-Tech Institute of Beijing, Beijing 100085, China.

Received: 2 September 2016 Accepted: 4 November 2016
Published online: 10 November 2016

References

1. Angaji MT, Ghiaee R (2015) Cavitational decontamination of unsymmetrical dimethylhydrazine waste water. J Taiwan Inst Chem Eng 49:142–7
2. Carp O, Huisman CL, Reller A (2004) Photoinduced reactivity of titanium dioxide. Prog Solid State Chem 32:33–177
3. Yu J, Dai G, Cheng B (2010) Effect of crystallization methods on morphology and photocatalytic activity of anodized TiO_2 nanotube array films. J Phys Chem C 114:19378–85
4. Pan JH, Lei Z, Wan IL, Xiong Z, Wang Q, Zhao XS (2011) Mesoporous TiO_2 photocatalytic films on stainless steel for water decontamination. J Virol 2:147–55
5. Zhang H, Guo LH, Wang D, Zhao L, Wan B (2015) Light-induced efficient molecular oxygen activation on a Cu(Ii)-grafted TiO_2/graphene photocatalyst for phenol degradation. ACS Appl Mater Interfaces 7:1816–23
6. Wang J, Li H, Zou C, Wang H, Li D (2014) Mesoporous TiO_2 thin films exhibiting enhanced thermal stability and controllable pore size: preparation and photocatalyzed destruction of cationic dyes. ACS Appl Mater Interfaces 6:1623–31
7. Chalasani R, Vasudevan S (2013) Cyclodextrin-functionalized Fe_3O_4@TiO_2: reusable, magnetic nanoparticles for photocatalytic degradation of endocrine-disrupting chemicals in water supplies. ACS Nano 7:4093–104
8. Guo X, Chen C, Song W, Xue W, Di W, Qin W (2014) CdS embedded TiO_2 hybrid nanospheres for visible light photocatalysis. J Mol Catal A Chem 387:1–6
9. Khanna A, Shetty VK (2014) Solar light induced photocatalytic degradation of reactive blue 220 (Rb-220) dye with highly efficient Ag@TiO_2 core–shell nanoparticles: a comparison with UV photocatalysis. Sol Energy 99:67–76
10. Yun JH, Hahn C, Liu B, Yang P (2012) Photoelectrochemical properties of TiO_2 nanowire arrays: a study of the dependence on length and atomic layer deposition coating. ACS Nano 6:5060–9
11. Yang L, Yu LE, Ray MB (2009) Photocatalytic oxidation of paracetamol: dominant reactants, intermediates, and reaction mechanisms. Environ Sci Technol 43:69–77
12. Daghrir R, Drogui P, Robert D (2013) Modified TiO_2 for environmental photocatalytic applications: a review. Ind Eng Chem Res 52:3581–99
13. Zhou H, Qu Y, Zeid T, Duan X (2012) Towards highly efficient photocatalysts using semiconductor nanoarchitectures. Energ Environ Sci 5:6732–43
14. Xu H, Ouyang S, Liu L, Reunchan P, Umezawa N, Ye J (2014) Recent advances in TiO_2-based photocatalysis. J Mater Chem A 2:12642–61
15. Baker DR, Kamat PV (2009) Photosensitization of TiO_2 nanostructures with CdS quantum dots: particulate versus tubular support architectures. Adv Funct Mater 19:805–11
16. Zhang AY, Wang WK, Pei DN, Yu HQ (2016) Degradation of refractory pollutants under solar light irradiation by a robust and self-protected ZnO/CdS/TiO_2 hybrid photocatalyst. Water Res 92:78–86
17. Das K, De SK (2009) Optical properties of the type-Ii core–shell TiO_2@CdS nanorods for photovoltaic applications. J Phys Chem C 113:3494–501
18. Xie Z, Liu X, Wang W, Wang X, Liu C, Xie Q et al (2014) Enhanced photoelectrochemical and photocatalytic performance of TiO_2 nanorod arrays/CdS quantum dots by coating TiO_2 through atomic layer deposition. nano energy 11:400–8
19. Xin G, Liu X, Zhu Z, Wang X, Zheng X (2016) Enhanced photoelectrochemical and photocatalytic behaviors of MFe_2O_4 (M=Ni, Co, Zn and Sr) modified TiO_2 nanorod arrays. Sci Rep 6:30543–554
20. Xie Z, Liu X, Wang W, Liu C, Li Z, Zhang Z (2014) Enhanced photoelectrochemical properties of TiO_2 nanorod arrays decorated with CdS nanoparticles. Sci Technol Adv Mater 15:055006–16
21. Robert TD, Laude LD, Geskin VM, Lazzaroni R, Gouttebaron R (2003) Micro-Raman spectroscopy study of surface transformations induced by excimer laser irradiation of TiO_2. Thin Solid Films 440:268–77
22. Ma HL, Yang JY, Dai Y, Zhang YB, Lu B, Ma GH (2007) Raman study of phase transformation of TiO_2 rutile single crystal irradiated by infrared femtosecond laser. Appl Surf Sci 253:7497–500
23. Wang ZQ, Gong JF, Duan JH, Huang HB, Yang SG, Zhao XN et al (2006) Direct synthesis and characterization of CdS nanobelts. Appl Phys Lett 89:033102–3
24. Mali SS, Desai SK, Dalavi DS, Betty CA, Bhosale PN, Patil PS (2011) CdS-sensitized TiO_2 nanocorals: hydrothermal synthesis, characterization, application. Photochem Photobiol Sci 10:1652–8
25. Wang S, Xu J, Ding H, Pan S, Zhang Y, Li G (2012) Facile synthesis of nitrogen self-doped rutile TiO_2 nanorods. Crystengcomm 14:7672–9
26. Cheng X, Yu X, Xing Z (2012) Characterization and mechanism analysis of N doped TiO_2 with visible light response and its enhanced visible activity. Appl Surf Sci 258:3244–8
27. Shang S, Jiao X, Chen D (2011) Template-free fabrication of TiO_2 hollow spheres and their photocatalytic properties. ACS Appl Mater Interfaces 4:860–5
28. Singh S, Khare N (2015) Reduced graphene oxide coupled CdS/$CoFe_2O_4$ ternary nanohybrid for enhanced photocatalytic activity and stability: a potential role of reduced graphene oxide as a visible light responsive photosensitizer. J Virol 77:4139–48
29. Li G, Wu L, Li F, Xu P, Zhang D, Li H (2013) Photoelectrocatalytic degradation of organic pollutants Via a CdS quantum dots enhanced TiO_2 nanotube array electrode under visible light irradiation. Nanoscale 5:2118–25
30. Bai H, Liu Z, Sun DD (2011) Hierarchical ZnO/Cu "Corn-Like" materials with high photodegradation and antibacterial capability under visible light. Phys Chem Chem Phys 13:6205–10
31. Li Y, Hwang DS, Lee NH, Kim SJ (2005) Synthesis and characterization of carbon-doped titania as an artificial solar light sensitive photocatalyst. Chem Phys Lett 404:25–9

32. Ren W, Ai Z, Jia F, Zhang L, Fan X, Zou Z (2007) Low temperature preparation and visible light photocatalytic activity of mesoporous carbon-doped crystalline TiO_2. Appl Catal B Environ 69:138–44
33. Wang M, Ioccozia J, Sun L, Lin C, Lin Z (2014) Inorganic-modified semiconductor TiO_2 nanotube arrays for photocatalysis. Energ Environ Sci 7:2182–202
34. Cho IS, Chen Z, Forman AJ, Dong RK, Rao PM, Jaramillo TF et al (2011) Branched TiO_2 nanorods for photoelectrochemical hydrogen production. Nano Lett 11:4978–84
35. Zhu G, Pan L, Xu T, Sun Z (2011) One-step synthesis of CdS sensitized TiO_2 photoanodes for quantum dot-sensitized solar cells by microwave assisted chemical bath deposition method. ACS Appl Mater Interfaces 3:1472–8
36. Gao X, Liu X, Zhu Z, Wang X, Xie Z (2016) Photoelectrochemical and photocatalytic properties of $NiFe_2O_4/TiO_2$ nanorod arrays. J Inorg Mate 31:935–42
37. Ryu J, Choi W (2004) Effects of TiO_2 surface modifications on photocatalytic oxidation of arsenite: the role of superoxides. Environ Sci Technol 38:2928–33
38. Jin S, Li Y, Xie H, Chen X, Tian T, Zhao X (2012) Highly selective photocatalytic and sensing properties of 2d-ordered dome films of nano titania and nano Ag^{2+} doped titania. J Mater Chem 22:1469–76
39. Yatmaz HC, Akyol A, Bayramoglu M (2004) Kinetics of the photocatalytic decolorization of an azo reactive dye in aqueous ZnO suspensions. Ind Eng Chem Res 43:6035–9
40. Liu Y, Xie C, Li J, Zou T, Zeng D (2012) New insights into the relationship between photocatalytic activity and photocurrent of TiO_2/WO_3 nanocomposite. Appl Catal A Gen 433–434:81–7
41. And MJ, Levanon H, Kamat PV (2003) Charge distribution between UV-irradiated TiO_2 and Gold nanoparticles: determination of shift in the fermi level. Nano Lett 3:353–8
42. Wood A, Giersig M, Mulvaney P (2001) Fermi level equilibration in quantum dot–metal nanojunctions. J Phys Chem B 105:8810–5
43. Zhang Y, Zhang N, Tang ZR, Xu YJ (2012) Improving the photocatalytic performance of graphene-TiO_2 nanocomposites via a combined strategy of decreasing defects of graphene and increasing interfacial contact. Phys Chem Chem Phys 14:9167–75
44. Jing L, Qu Y, Wang B, Li S, Jiang B, Yang L et al (2006) Review of photoluminescence performance of nano-sized semiconductor materials and its relationships with photocatalytic activity. Sol Energy Mater Sol Cells 90:1773–87
45. Dong W, Pan F, Xu L, Zheng M, Sow CH, Wu K et al (2015) Facile synthesis of CdS@TiO_2 core–shell nanorods with controllable shell thickness and enhanced photocatalytic activity under visible light irradiation. Applied Surface Science 349:279–86
46. Zhan P, Xie Z, Li Z, Wang W, Zhang Z, Li Z et al (2013) Origin of the defects-induced ferromagnetism in Un-doped ZnO single crystals. Appl Phys Lett 102:071914
47. Li X, Wang J, Yong M, Bian Z (2016) TiO_2 mesocrystal with exposed (001) facets and CdS quantum dots as an active visible photocatalyst for selective oxidation reactions. Appl Catal B Environ 187:115–21